Electronic Supplementary Material (ESI) for Physical Chemistry Chemical Physics

The role of CH-π interaction in the charge transfer properties in tris(8-hydroxyquinolinato)aluminum(III)

Supporting information

Bo-Chao Lin,[a], Cheu-Pyeng Cheng[b,*], Zhi-Qiang You[a,c], and Chao-Ping Hsu[a*]

[a] *Institute of Chemistry, Academia Sinica,*

128 Section 2 Academia Road, Nankang, Taipei 11529, Taiwan

[b] *Department of Chemistry, National Tsing Hua University,*

101 Section 2 Kuang-Fu Road, Hsinchu 30031, Taiwan

[c] *Taiwan International Graduate Program, Academia Sinica,*

128 Section 2 Academia Road, Nankang, Taipei 11529, Taiwan

CONTENTS

In this supporting material, we include additional methodological details of our computation and analyses first. The results from analyzing crystal structures, and additional results of quantum chemistry calculations on binding energy are included in the following sections.

I. METHODS

A. Additional crystal structures studied

Two crystal structures of five-coordinated Al(III) complexes were also surveyed and discussed in this supplementary section. They are bis(2-methylquinolin-8-olato-$\kappa^2 N,O$)-(6-phenyl-2-naphtholato-κO)-aluminium(III) (GEVGOE[1]), and bis(2,4-Dimethyl-8-quinolinolato-$\kappa^2 N,O$)-(2,6-diphenylphenolato-κO)-aluminium(III) (PIYGIO[2]).

B. Further details of molecular mechanical calculations

Molecular mechanics is frequently seen to simulate the AlQ_3 intermolecular structures[3–5]. With a mechanical force field, we can simulate a cluster of AlQ_3 molecules and obtain the intermolecular structure for further analysis. It is a quick and low-cost way to estimate binding energies. It also allows us to decompose the intermolecular binding energies into

van der Waals and electrostatic interactions, which is not directly available in the quantum calculation. In the present work, we employed the UFF force field and RESP charges in the molecular mechanics calculations. The program "analyze" in Tinker version 4.2[6] was to calculate the intermolecular interaction energies. As seen in FIG. 1, there exists a very good correlation between the binding energies calculated by the classical force field and by quantum mechanics. The mean and standard deviation of this estimated binding energy and the actual quantum binding energy was 0.39 and 0.45 kcal/mol, respectively, with the maximum deviation being 1.74 kcal/mol.

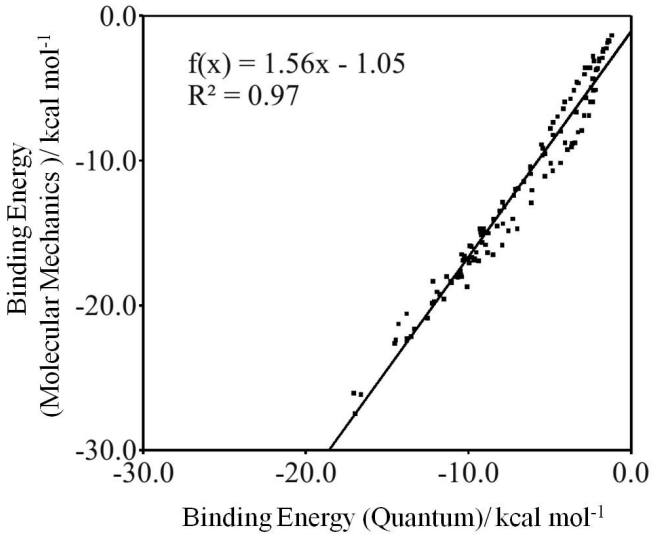

FIG. 1. The correlation between binding energies calculated using quantum mechanics at the TRIM-MP2/6-31G* level and the classical force field, UFF/RESP, between pairs of AlQ_3s derived from crystal structures and model pairs.

C. Calculation of Dipole moment

We had optimized the geometries for the three molecules AlQ_3, and the two AlQ_3 analogs studied previously,[7], tris(4-hydroxy-8-methyl-1,5-naphthyridinato)aluminum ($AlmND_3$) and tris(4-hydroxy-2,8-dimethyl-1,5-naphthyridinato)aluminum ($AlmmND_3$), in their neutral, anionic, and cationic states, respectively, in order to estimate the change of dipole moments in the ionic states. The calculations were performed at (U)B3LYP/6-31G* level with a developmental version of Q-Chem.[8]

II. SUPPLEMENTARY RESULTS

A. Variations in the frontier molecular orbitals of AlQ_3

The CT coupling is essentially an off-diagonal Fock matrix element between the two frontier molecular orbitals (FMOs) involved in the CT process, i.e, the highest occupied MO (HOMO) for hole transfer (HT) or the lowest unoccupied MO (LUMO) for electron transfer (ET) of the donor and acceptor fragments. AlQ_3 has three chemically identical ligands, with their π and π^* orbitals near the band gap. Since the three π or π^* orbitals are similar in their energies, the MOs of an AlQ_3 near HOMO (or LUMO) are essentially linear combination of the three π (or π^*) orbitals, with their MO energies nearly degenerate. A small fluctuation can easily change the relative composition of the HOMOs or LUMO.

With the sensitivity of the MO population to a small perturbation, a large change in the CT coupling between two AlQ_3 molecules may be seen. In TABLE I we list the Al-O and Al-N bond lengths as representative parameters of AlQ_3 structures in different crystals. Such structural variation affects energies and compositions of the FMOs. As a result, the distributions of HOMO and LUMO population in different structures are varied. The most delocalized and the most localized HOMOs and LUMOs are shown in FIG. 2. It is seen that the compositions of FMOs are mainly composed of the π and π^* orbitals, the HOMO and LUMO of ligands, but the fraction in each ligand is sensitive to the structural differences among crystals. It has been reported that different level of computation would also lead to different MO locations[4]. Therefore, the electronic coupling derived from the ionic states can be varied to a large extent but the basic properties remain in the π and π^* orbitals of a Q ligands.

B. The conformations of *mer*-AlQ_3 pairs

There are three planar Q ligands in an AlQ_3 molecule, each with two possible sides to form a π-π interaction. The steric hindrances for the six π-π stacking sites are different for a *mer*-AlQ_3. Possible ligand-ligand contacts for the six stacking sites are depicted in FIG. 3 (A)–(F).

From FIG. 3, it can be seen that out of the total 6 possible π-π interaction sites, three of them have a second ligand to form a CH-π interaction with the incoming ligand as seen

TABLE I. Al-N and Al-O bond lengths (in units of Å) in AlQ_3 crystals.

CSD refcode	Qa		Qb		Qc	
	Al-N	Al-O	Al-N	Al-O	Al-N	Al-O
HQUALA01	2.048	1.841	2.074	1.850	2.026	1.881
ISIJAV	2.042	1.867	2.062	1.888	2.036	1.862
ISIJOJ	2.045	1.861	2.077	1.881	2.027	1.875
JIWLAC	2.034	1.848	2.073	1.845	2.028	1.857
POVWEC	2.034	1.850	2.077	1.859	2.032	1.862
QATMED	2.060	1.857	2.059	1.857	2.058	1.856
QATMON	2.050	1.851	2.087	1.860	2.017	1.857
QATMON01	2.054	1.852	2.051	1.851	2.052	1.851
QATMON03(Al1)	2.021	1.840	2.048	1.869	2.007	1.869
QATMON03(Al2)	2.039	1.851	2.033	1.864	2.007	1.866
QATMON03(Al3)	2.037	1.850	2.038	1.851	2.006	1.868
XADHUG	2.039	1.838	2.067	1.860	2.038	1.868
XADJAO	2.054	1.834	2.080	1.867	2.027	1.879

in FIG. 3 (A)-(F). The second ligands offering the π electrons involved in CH-π interaction are labeled with yellow shaded rectangles in FIG. 3. In FIG. 3 (G) and (H), we overlaid the the structure of the inter-ligand configurations, regardless of the cases for Qa, Qb, or Qc. It can be seen that there are two different orientations for the second ligand offering CH-π interaction sites (shaded in yellow in FIG. 3 in panel (B) versus those in panels (D) and (F)). Therefore, the intermolecular contact in Qa (FIG. 3 (B)) is quite different from those for Qb and Qc. As a result, in FIG. 3 (G) the overlaid picture includes a three-ring object that is a superposition of the two orientations of the second CH-π interacting ligand.

An interesting and potentially important observation for the structures is that, instead of a full π-π overlap, the incoming ligands are mostly shifted toward where a CH-π interaction is available, which is toward an overlap over the pyridyl ring in the π-π interaction. Therefore, we propose that the CH-π interaction bias the position of the incoming ligand towards pyridyl-pyridyl contact, and away from phenoxide-phenoxide contact region. The CH-π interacting ligands also block the incoming ligands and prevent the advanced π-π overlap.

The other three π-π interaction sites, without CH-π interaction, are either in a relatively open space (such as the cases for Qa and Qc, FIG. 3 (A) and (E)) that allows a large π-π overlap, or in a very crowded space that does not allow any significant π-π interaction (Qb, FIG. 3 (C)). Those configurations are less common. In the crystal structures we surveyed,

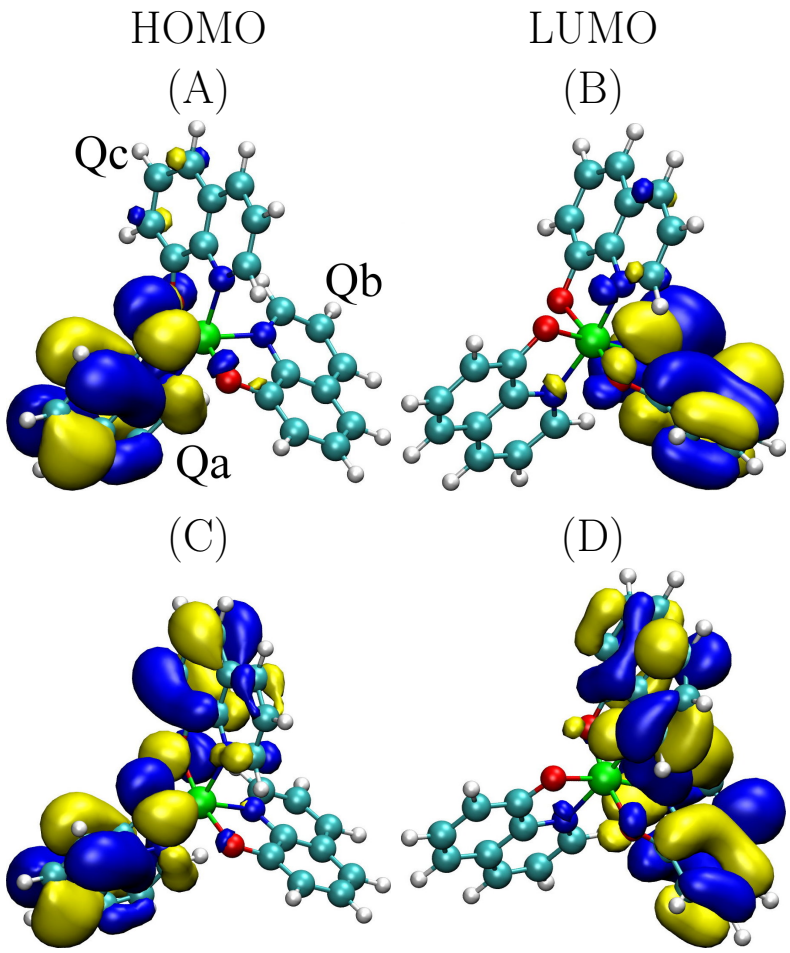

FIG. 2. The most localized ((A) and (B)) and delocalized ((C) and (D)) FMOs. Panels (A) and (C) are for HOMOs, and in panels (B) and (D) are LUMOs, respectively. Shown are the contour surfaces depicted at an isovalue of 0.02 a.u.

we have only seen 4 such occurrences.

There are 28 different parallel π-π ligand contacts configurations. We further classify the 28 π-π configurations into the six contact types, four with CH-π interaction involving Qa//Qa, Qb//Qb, Qa//Qb, and Qc//Qc (FIG. 4 (A), (B), (D), and (F)), and two without CH-π interaction involving Qa//Qc, and Qc//Qc (FIG. 4 (C) and (E)), with the representative examples shown in FIG. 4. We have use a notation "Qa//Qb" to denote a parallel π-π interaction, where Qa and Qb from the two AlQ_3 molecules are in π-π contact.

There exist several other interesting interactions in conformations seen in crystal structures but without an apparent CH-π interaction. In Qc//Qc, it is seen that there exist a pair of CH-O interaction between the H_4 and H_5 atoms in Qc and the O atom in Qa (FIG. 4 (C)). The case of Qa//Qc is quite special since it is composed of two identical AlQ_3

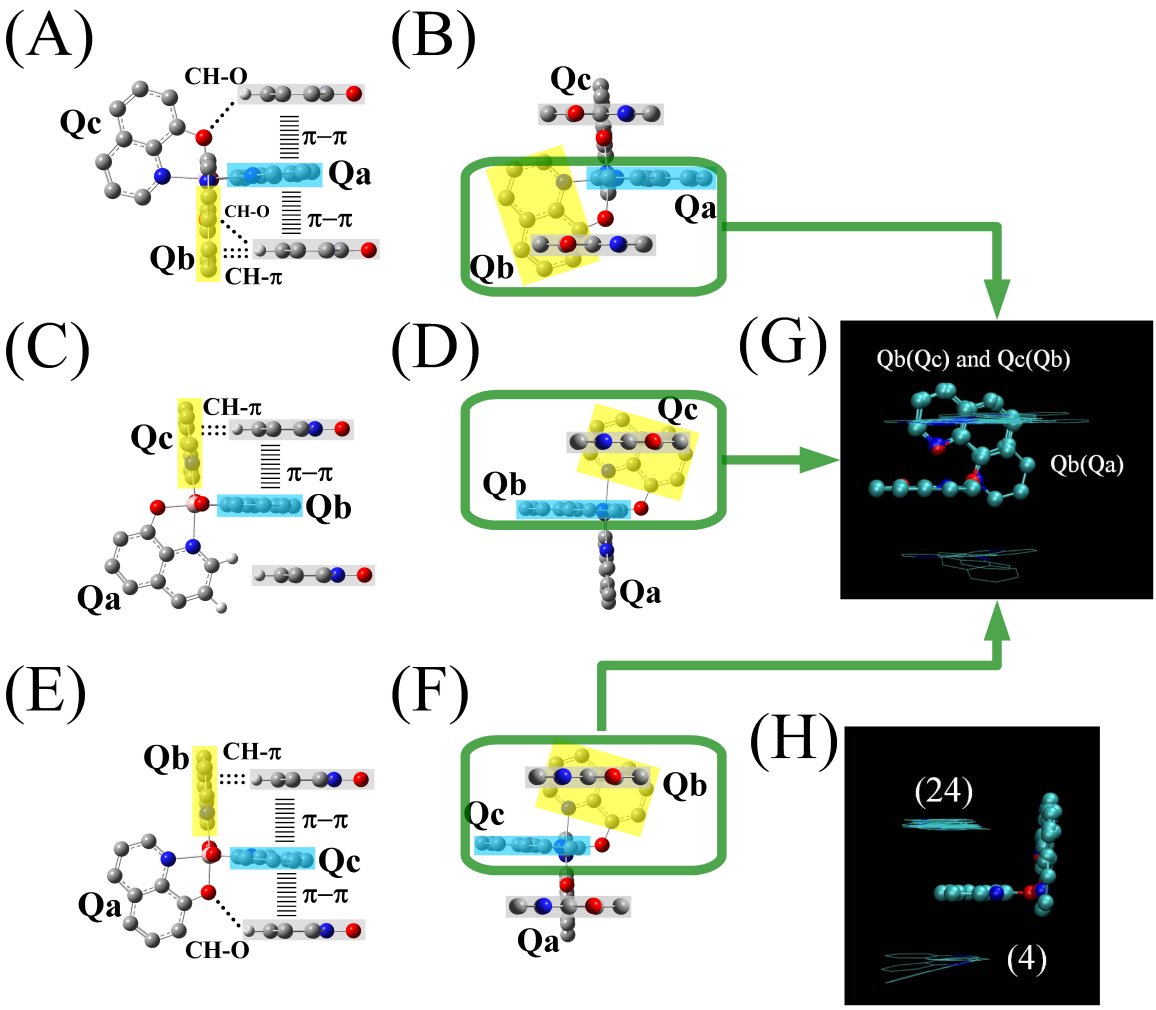

FIG. 3. (A)-(F) Possible interaction sites that allows a π-π interaction between two Q ligands. Shown are one central AlQ_3 and one ligand from the second AlQ_3. In (A) and (B) are for interaction with Qa, (C) and (D), Qb, and (E) and (F), Qc, from two different viewing angles. In there panels, the blue shaded rectangles denote the ligand of the central molecule forming π-π interaction, the yellow shaded rectangles mark the π electron donor for the CH-π interaction, and the gray shaded rectangles mark the incoming ligands. In (G) and (H) are the overlaid structure of the 28 bimolecular structures with parallel π-π contact derived from crystal structures, regardless of Qa, Qb, or Qc. The two ligands involved (π-π and CH-π) in the central AlQ_3 are shown in the stick-and-ball model. The Q ligands (of the second AlQ_3) that form π-π interaction with the central molecule are shown in the thin wire model. For the sake of clarity, the rest of the molecules was omitted in these panels. The numbers in parentheses in (H) are the number of structures found in crystals.

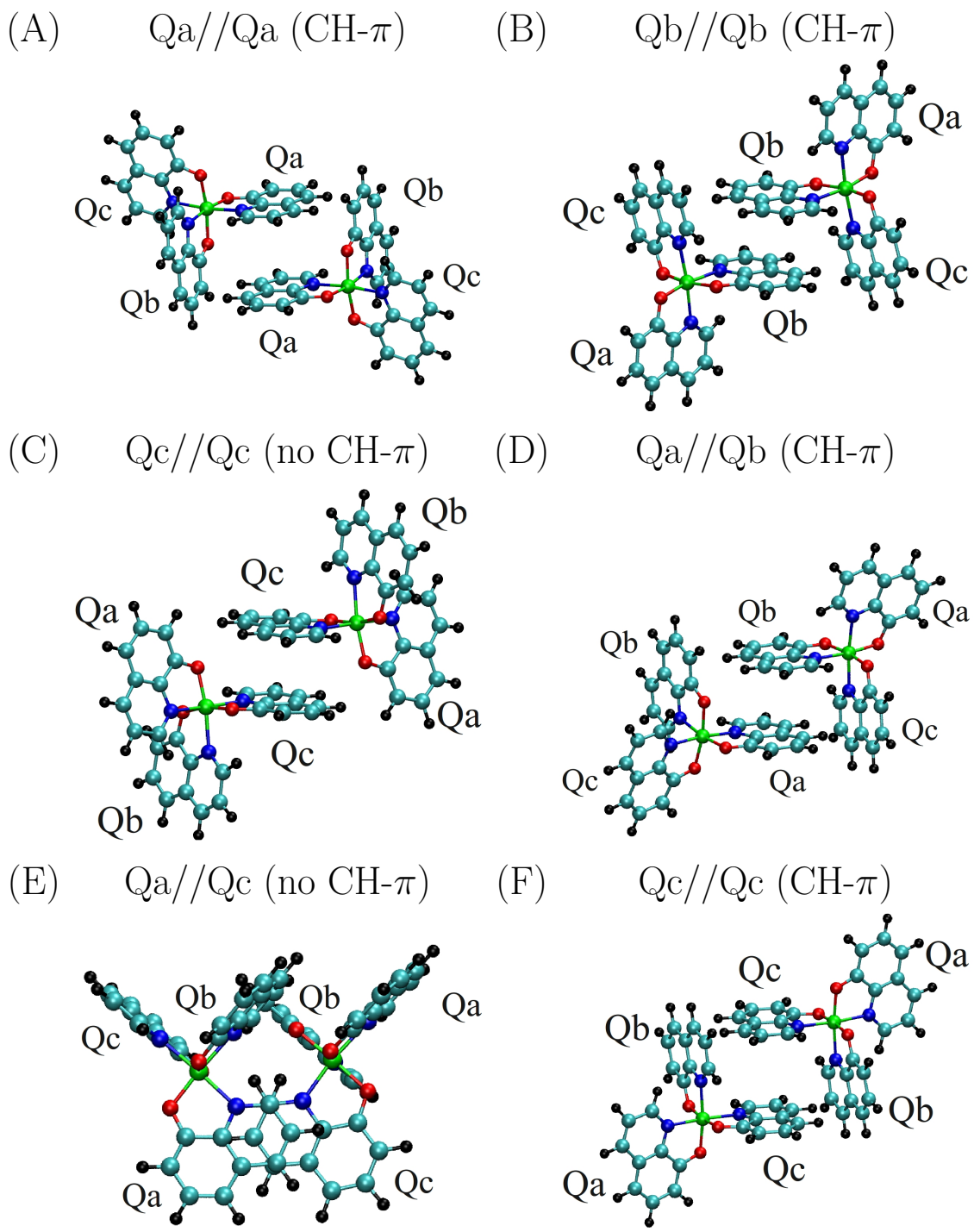

FIG. 4. Representative structures for the six contact types. Shown are from in crystal structure QATMON (A-C) and QATMON03 (D-F) with their corresponding notation.

molecules, instead of a pair of enantiomers as in all other cases. In FIG. 4 (E), it can be seen that there exists a π-π interactions in Qa//Qc between the pyridyl moiety of Qa for the AlQ_3 at the left-hand side (LHS) and the pyridyl moiety in the Qc from the right-hand side (RHS) AlQ_3, and the two parallel ligands have a large angle between in their long axes, which is very different from other cases. There are other weak π-π interactions in this case, i.e., between the pyridyl ring in the Qb (LHS) and the phenoxide ring in the Qa (RHS), and between Qc(LHS) and Qb(RHS). In addition, it may not be clearly seen in the 2-dimensional projections, there are three CH-O interactions (between H_2 and O) between Qa (LHS) and Qa (RHS), Qb(LHS) and Qb(RHS), and Qc(RHS) and Qc(LHS), respectively (FIG. 4 (E)).

For these π-π and CH-π interacting AlQ_3 pairs, we estimated their relative displacements (Δx, Δy, and Δz as defined in FIG. 3 (A) of the main text) for the two parallel ligands, according to the method described in the method section, and the results are listed in TABLE II. The binding energies from both quantum mechanics and force field calculations are also listed. The relative displacements are also included in FIG. 3 (E) and (F) in the main text. It is seen that the Δx coordinates are larger than zero for all the 24 structures with CH-π interaction, indicating a clear bias towards pyridyl-pyridyl contact.

C. The π-π and CH-π interaction in five-coordinated similar molecules

We have discussed on other MQ_3 molecules, as well as six-coordinated molecules with two Q or similar ligands in the main text. Another class of molecules we examined are five-coordinated molecules with two Q or similar ligands. The two Q ligands in these molecules are well separated, making CH-π interaction unavailable for the π-π interacting ligands. In two five-coordinated Al(III) complexes, bis(2-methylquinolin-8-olato-$\kappa^2 N,O$)-(6-phenyl-2-naphtholato-κO)-aluminium(III) and bis(2,4-Dimethyl-8-quinolinolato-$\kappa^2 N,O$)-(2,6-diphenylphenolato-κO)-aluminium(III)[1,2], the π-π interaction is no longer coupled with CH-π interaction, and the π-π overlaps found in crystal structures are no longer biased towards pyridyl-pyridyl contact. The contrasting differences between these molecules and AlQ_3 shows the importance of CH-π interaction in the bias towards pyridyl-pyridyl contact. From this result, we also note the importance in the relative position of π-conjugated fragments for the formation of CH-π interaction. As pointed out above, we found that CH-π interaction can bias the π-π stack position towards pyridyl-pyridyl contact and enhances

TABLE II. Intermolecular binding energies and structural characteristics for the AlQ_3 dimers with π-π interaction.

CSD refcode	Al-Al	Force field[a]			Quantum binding energy[b]			Stacking structure[c]			
	Distance	Total	vdW	Coul	Total	π-π	CH-π	Contact type[d]	Δx	Δy	Δz
With CH-π interaction											
HQUALA01	8.426	-21.62	-15.79	-5.83	-13.35	-5.24	-4.69	Qa//Qa	1.9	0.9	3.4
HQUALA01	8.723	-16.57	-14.99	-1.58	-10.28	-4.29	-4.65	Qc//Qc	3.2	0.9	3.5
ISIJAV	8.351	-20.55	-14.49	-6.06	-13.82	-5.29	-4.37	Qa//Qa	1.6	0.9	3.3
ISIJAV	8.657	-18.42	-16.40	-2.01	-11.07	-4.63	-4.90	Qc//Qc	2.6	0.9	3.4
ISIJOJ	8.312	-22.38	-16.70	-5.68	-14.49	-5.39	-4.92	Qa//Qa	1.6	0.8	3.3
ISIJOJ	8.621	-18.01	-16.30	-1.70	-10.43	-5.08	-4.14	Qc//Qc	2.1	0.9	3.5
JIWLAC	8.488	-22.14	-16.51	-5.62	-13.55	-5.02	-5.37	Qa//Qa	2.0	1.0	3.4
JIWLAC	8.793	-16.65	-15.06	-1.59	-9.79	-4.02	-4.65	Qc//Qc	3.2	0.9	3.6
POVWEC	8.476	-22.43	-16.40	-6.03	-13.82	-5.70	-6.67	Qa//Qa	2.1	0.9	3.3
POVWEC	8.780	-16.88	-15.25	-1.63	-10.37	-4.58	-4.89	Qc//Qc	3.3	0.9	3.5
QATMED	8.439	-18.31	-12.89	-5.42	-12.20	-5.91	-5.32	Qa//Qa	2.1	0.9	3.4
QATMED	8.863	-16.87	-15.57	-1.30	-9.68	-4.01	-5.48	Qc//Qc	3.2	1.3	3.7
QATMON	9.112	-14.99	-10.62	-4.37	-8.80	-2.74	-4.12	Qa//Qa	4.2	1.0	3.4
QATMON	8.957	-18.69	-18.37	-0.32	-10.10	-4.62	-3.45	Qb//Qb	0.4	1.2	3.4
QATMON01	9.009	-14.86	-10.86	-4.00	-9.11	-3.78	-3.96	Qa//Qa	3.5	1.3	3.5
QATMON01	8.931	-15.85	-14.25	-1.60	-9.94	-4.30	-3.82	Qb//Qb	3.2	0.8	3.6
QATMON03(Al1)	8.814	-20.87	-16.62	-4.25	-12.54	-4.63	-5.24	Qa//Qb	2.5	1.1	3.4
QATMON03(Al1)	8.954	-19.55	-15.80	-3.75	-11.52	-4.29	-4.82	Qa//Qb	2.2	1.5	3.4
QATMON03(Al2)	8.954	-12.86	-10.63	-2.23	-7.92	-2.11	-4.40	Qc//Qc	4.8	0.5	3.8
QATMON03(Al3)	8.644	-14.68	-9.49	-5.19	-9.30	-1.86	-5.16	Qa//Qa	5.8	-0.6	3.4
XADHUG	8.413	-22.26	-16.29	-5.97	-13.79	-4.94	-5.23	Qa//Qa	2.1	0.8	3.4
XADHUG	8.813	-18.05	-16.39	-1.67	-10.66	-4.40	-5.10	Qc//Qc	3.0	1.1	3.4
XADJAO	8.407	-22.60	-16.52	-6.08	-14.56	-5.30	-5.45	Qa//Qa	1.9	0.8	3.4
XADJAO	8.648	-18.00	-16.26	-1.74	-10.73	-4.40	-5.01	Qc//Qc	3.0	0.9	3.4
Without CH-π interaction[e]											
QATMON	8.101	-21.25	-15.84	-5.41	-14.32			Qc//Qc	1.2	0.4	3.4
QATMON03(Al1)	6.256	-26.04	-18.63	-7.41	-17.06			Qa//Qc			
QATMON03(Al1)	6.340	-27.45	-19.72	-7.73	-16.98			Qa//Qc			
QATMON03(Al2)	6.165	-26.14	-18.60	-7.54	-16.63			Qa//Qc			

[a] Binding energy estimated using UFF/RESP, in the units of kcal/mol; "vdW" stands for van der Waals interaction, and "Coul." denotes electrostatic interaction from RESP charges.

[b] Quantum mechanical binding energy calculated via TRIM-MP2/6-31G*. In the π-π and CH-π columns are binding energies for the corresponding pair of ligands. The H atoms were optimized in dimers before the binding energy computation.

[c] The definition of Δx, Δy, and Δz are illustrated in FIG. 3(A) of the main text, in the units of Å.

[d] Contact types are as illustrated in FIG. 4.

[e] In this section, we did not include the shift values Δx, Δy, and Δz for Qa//Qc contact type because it is quite different from the typical structure shown in FIG. 3(A) of the main text, as seen in FIG. 4 (E).

the electronic interaction for ET. If the π-conjugated fragments are well-separated in space, CH-π interaction is no longer formed and the bias for a relative position of the two molecules does not exist.

D. Dipole moments and their changes

The change in dipole moment has been regarded as a major factor that contribute to the difference in electron and hole mobilities in AlQ_3 since it leads to a difference in the site energy disorder[3,5,9]. The dependence between charge mobility and the site energetic disorder is written as[10]

$$\mu(\sigma, \Sigma, E) = \mu_0 \exp\left[-\left(\frac{2}{3}\sigma\right)^2\right] \begin{cases} \exp\left(C\left(\sigma^2 - \Sigma^2\right)E^{1/2}\right); & \Sigma \geq 1.5, \\ \exp\left(C\left(\sigma^2 - 2.25\right)E^{1/2}\right); & \Sigma < 1.5, \end{cases} \tag{2.1}$$

where σ is the standard deviation of site energy distribution, Σ is the standard deviation in the off-diagonal matrix elements, both are in the units of thermal energy, k_BT. μ_0 is a prefactor for the mobility, E is the electric field strength, and C is a fitted constant. In an amorphous film, the σ is dependent on the dipole moment:[11]

$$\sigma = \frac{2.35de}{\epsilon a^2}, \tag{2.2}$$

where a is the intersite distance, ϵ is the dielectric constant of matter, d is the dipole moment, and e is the charge of an electron. It's seen that σ is proportional to the size of dipole moment. We have calculated the dipole moments for the three molecules AlQ_3, $AlmND_3$, and $AlmmND_3$. The optimized geometries and the dipole moments are included in FIG. 5. The calculated dipole moments of neutral molecules are listed in TABLE III.

From TABLE III, it is seen that neutral AlQ_3 has the largest dipole moment and $AlmmND_3$ has the smallest one. According to Eq. 2.2, the energy disorder of $AlmmND_3$ would be the smallest and its mobility is expected to be the largest. However, the experimental electron mobilities of $AlmmND_3$ is smaller than the other analog $AlmND_3$.[7]

The dipole moment change upon ionization is also reported as a factor that determine the size of σ[9]. The calculated dipole moment change are included in TABLE III. It is seen that the anionic $AlmmND_3$ now has a larger dipole moment change from the neutral state,

TABLE III. Calculated dipole moments of AlQ_3, $AlmND_3$, and $AlmmND_3$, and their dipole moment change in anions and cations.

Molecules	Dipole moment[a]	Dipole moment change[b]	
	Neutral	Anion	Cation
AlQ_3	4.36	4.89	5.16
$AlmND_3$	4.02	4.97	4.84
$AlmmND_3$	3.60	5.37	4.81

[a] Computational results at the level of B3LYP/6-31g*, in units of Debye.
[b] Dipole difference from the neutral state to the corresponding ionic states, in units of Debye.

as compared to that in AlQ_3. However the electron mobilities for $AlmmND_3$ and AlQ_3 are similar in their order of magnitude. In addition, the dipole change in anionic $AlmmND_3$ is larger than its cationic dipole change, but $AlmmND_3$ has a larger electron mobility than hole mobility and this is opposite to the experimental results.

The discrepancy in dipole moment change and charge mobility is seen in comparisons of two similar molecules, as well as the electron and hole mobilities in the same molecule. Therefore we believe that there exist other factors, such as the electronic coupling factor, contributing to the charge transporting property of AlQ_3 and similar molecules.

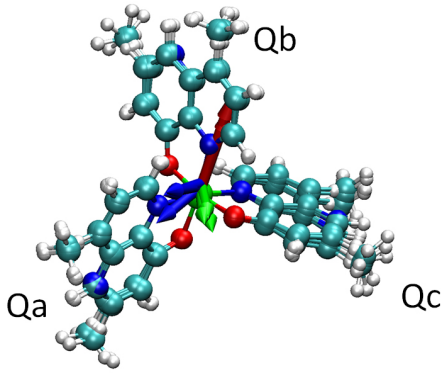

FIG. 5. Optimized geometries and dipole moments for AlQ_3, $AlmND_3$, and $AlmmND_3$, in their neutral, cationic, and anionic states. The nine geometries are superimposed to show their structural similarity. The dipole moments for neutral, anionic, and cationic states are shown with red, blue, and green arrows, respectively.

E. Effects of solvent in the crystals

The parallel stacking configurations are more versatile in solvent-free AlQ_3 crystals than in crystals with solvents. There are six different contact types (as shown in FIG. 4) in the solvent-free crystals (QATMON and QATMON03), but only two of them (Qa//Qa and Qc//Qc) are found in crystals with solvents. Similarly, in MQ_3 crystals with solvents,[12–23] only Qa//Qa and Qc//Qc contacts are seen. To the best of our knowledge, Qb//Qb and Qc//Qc contacts are only seen in solvent-free MQ_3 crystals, such as solvent-free AlQ_3, GaQ_3 and InQ_3 crystals[24–26].

Even though the preferences of stacking configurations are different in between crystals with and without solvents, the effect of CH-π interaction and the resulting preference of pyridyl-pyridyl overlap are seen in all cases.

---

* E-mail: cpcheng@mx.nthu.edu.tw; cherri@sinica.edu.tw

[1] M. Rajeswaran, D. W. Place, V. W. Bakos, J. C. Deaton, C. T. Brown, and W. C. Lenhart, *Acta Cryst.*, 2007, **E63**, m54–m56.

[2] J. C. Deaton, D. W. Place, C. T. Brown, M. Rajeswaran, and M. E. Kondakova, *Inorg. Chim. Acta*, 2008, **361**, 1020–1035.

[3] Y. Nagata and C. Lennartz, *J. Chem. Phys.*, 2008, **129**, 034709.

[4] A. Lukyanov, C. Lennartz, and D. Andrienko, *Phys. Status Solidi A*, 2009, **206**, 2737–2742.

[5] J. J. Kwiatkowski, J. Nelson, H. Li, J.-L. Brédas, W. Wenzel, and C. Lennartz, *Phys. Chem. Chem. Phys.*, 2008, **10**, 1852–1858.

[6] Tinker: Software tools for molecular design, version 4.2. J. W. Ponder; St. Louis, MO, 2004.

[7] S.-H. Liao, J.-R. Shiu, S.-W. Liu, S.-J. Yeh, Y.-H. Chen, C.-T. Chen, T. J. Chow, and C.-I. Wu, *J. Am. Chem. Soc.*, 2009, **131**, 763–777.

[8] Y. Shao, L. F. Molnar, Y. Jung, J. Kussmann, C. Ochsenfeld, S. T. Brown, A. T. Gilbert, L. V. Slipchenko, S. V. Levchenko, D. P. O'Neill, R. A. DiStasio Jr, R. C. Lochan, T. Wang, G. J. Beran, N. A. Besley, J. M. Herbert, C. Yeh Lin, T. Van Voorhis, S. Hung Chien, A. Sodt, R. P. Steele, V. A. Rassolov, P. E. Maslen, P. P. Korambath, R. D. Adamson, B. Austin, J. Baker, E. F. C. Byrd, H. Dachsel, R. J. Doerksen, A. Dreuw, B. D. Dunietz, A. D. Dutoi, T. R. Furlani,

S. R. Gwaltney, A. Heyden, S. Hirata, C.-P. Hsu, G. Kedziora, R. Z. Khalliulin, P. Klunzinger, A. M. Lee, M. S. Lee, W. Liang, I. Lotan, N. Nair, B. Peters, E. I. Proynov, P. A. Pieniazek, Y. Min Rhee, J. Ritchie, E. Rosta, C. David Sherrill, A. C. Simmonett, J. E. Subotnik, H. Lee Woodcock III, W. Zhang, A. T. Bell, A. K. Chakraborty, D. M. Chipman, F. J. Keil, A. Warshel, W. J. Hehre, H. F. Schaefer III, J. Kong, A. I. Krylov, P. M. W. Gill, and M. Head-Gordon, *Phys. Chem. Chem. Phys.*, 2006, **8**, 3172–3191.

[9] Y. Nagata, *ChemPhysChem*, 2010, **11**, 474–479.

[10] H. Bässler, *Phys. Status Solidi B*, 1993, **175**, 15–56.

[11] R. L. Martin, J. D. Kress, I. H. Campbell, and D. L. Smith, *Phys. Rev. B*, 2000, **61**, 15804–15811.

[12] H. Schmidbaur, J. Lettenbauer, D. L. Wilkinson, G. Muller, and O. Kumberger, *Z. Naturforsch., B: Chem. Sci.*, 1991, **46**, 901–911.

[13] N. Korber, B. Achour, and F. Nepveu, *J. Chem. Crystallogr.*, 1994, **24**, 685–688.

[14] R.-G. Xiong, X.-Z. You, Q.-J. Wu, and X.-Y. Huang, *Acta Cryst.*, 1995, **C51**, 1978–1980.

[15] Y. Wang, W. Zhang, Y. Li, L. Ye, and G. Yang, *Chem. Mater.*, 1999, **11**, 530–532.

[16] D.-X. Li, D.-J. Xu, and Y.-Z. Xu, *Acta Cryst.*, 2003, **E59**, m271–m272.

[17] G. Chen, *Acta Cryst.*, 2006, **E62**, m3383–m3384.

[18] L. Pech, Y. A. Bankovsky, A. Kemme, and J. Lejejs, *Acta Cryst.*, 1997, **C53**, 1043–1045.

[19] R. Hems and M. F. Mackay, *J. Cryst. Mol. Struct.*, 1975, **5**, 227–245.

[20] S. Shanmuga Sundara Raj, I. A. Razak, H.-K. Fun, P.-S. Zhao, F. Jian, X. Yang, L. Lu, and X. Wang, *Acta Cryst.*, 2000, **C56**, e130–e131.

[21] M. J. Manos, A. J. Tasiopoulos, C. Raptopoulou, A. Terzis, J. D. Woollins, A. M. Z. Slawin, A. D. Keramidas, and T. A. Kabanos, *J. Chem. Soc., Dalton Trans.*, 2001, pp. 1556–1558.

[22] D.-X. Li, D.-J. Xu, J.-M. Gu, and Y.-Z. Xu, *Acta Cryst.*, 2003, **E59**, m543–m545.

[23] J. G. Malecki, M. Jaworska, R. Kruszynski, and J. Klak, *Polyhedron*, 2005, **24**, 3012–3021.

[24] M. Brinkmann, G. Gadret, M. Muccini, C. Taliani, N. Masciocchi, and A. Sironi, *J. Am. Chem. Soc.*, 2000, **122**, 5147–5157.

[25] M. Rajeswaran and V. V. Jarikov, *Acta Cryst.*, 2004, **E60**, m217–m218.

[26] L. S. Sapochak, A. Ranasinghe, H. Kohlmann, K. F. Ferris, and P. E. Burrows, *Chem. Mater.*, 2004, **16**, 401–406.